PHYSICAL REVIEW B VOLUME 5, NUMBER 2 15 JANUARY 1972

Radiation-Produced Absorption Bands in Silicon: Piezospectroscopic Study of a Group-V Atom-Defect Complex*

C. S. Chen† and J. C. Corelli
Department of Nuclear Science and Engineering, Rensselaer Polytechnic Institute, Troy, New York 12181

and

G. D. Watkins
General Electric Research & Development Center, Schenectady, New York 12301
(Received 17 June 1971)

A series of sharp new infrared-absorption bands produced by high-energy-electron irradiation in phosphorus- and arsenic-doped float-zone-refined silicon is reported. In P-doped silicon, the dominant band is at 1150 cm^{-1}, with associated weaker bands at 1310, 970, 1000, 1025, 1040, and 1450 cm^{-1}. In As-doped silicon, the corresponding bands are at 1260 cm^{-1} and 1480, 1080, 1110, 1135, 1160, and 1650 cm^{-1}. The spectra recover in both materials at ~140 °C. Uniaxial-stress studies of these bands in oriented single crystals with polarized light are described. The results cannot be fit to the usual "piezospectrospic" classification of Kaplyanskii and Runciman. A model is presented which identifies the spectra as electronic transitions from the orbital singlet ground state of a single anistropic donor defect to a manifold of bound large-orbit effective-mass excited states. Extension of the Kaplyanskii classification to include the accidental degeneracy inherent in the effective-mass excited states in silicon explains the stress results. The symmetry of the defect is deduced to be monoclinic II. It is deduced that one or more group-V atoms are involved in the defect, but a microscopic identification of the defect is not possible.

I. INTRODUCTION

In the past decade the use of spectroscopic probes to study radiation effects in silicon has given detailed knowledge of the structure, symmetry, and chemical makeup of some of the defects responsible for the induced property changes. In particular, the use of electron paramagnetic resonance (EPR)[1,2] and infrared (ir) spectroscopy[3–10] have allowed detailed models to be proposed which depict some of the simpler defect complexes.

In this paper, we report a series of sharp new ir-absorption bands in the 7- to 10-μ region[11] produced by electron irradiation of phosphorus- and arsenic-doped float-zone-refined silicon. The band positions are different in the two materials. However, the number of lines and their relative spacings and intensities are highly similar and we conclude that the two sets of spectra arise from a similar defect and that the group-V atom is directly involved in the defect.

Detailed studies of the production and annealing behavior of the bands will be presented. Also explored is the Fermi-level dependence and the role of the initial group-V atom doping concentration on the intensity of the bands produced.

The bands are found to exhibit well-resolved shifts and splittings under the influence of externally applied uniaxial stress. The stress effects are found to be qualitatively similar for the two sets of spectra and a detailed study of the orientation dependence of these effects with polarized light will be described. In order to explain the observed stress results, we find it necessary to extend the treatments of Kaplyanskii[12,13] and Runciman[14] to include the case where accidental degeneracy exists in the excited states. We show that in a semiconductor, such as silicon, the multivalleyed character of the conduction-band minima leads naturally to the required accidental degeneracy. With this analysis it is possible to deduce the symmetry of the defect and to understand the nature of the electronic transitions involved. The detailed make up of the defect, however, remains undetermined.

II. EXPERIMENTAL METHODS

The silicon single-crystal materials used in these experiments were all float zone refined. Typical sample dimensions were $2\times 0.2\times 0.3$ cm^3, in which the long dimension was either a $\langle 111\rangle$, $\langle 100\rangle$, or $\langle 110\rangle$ orientation. The crystal orientation was determined either by x-ray backreflection Laue technique or by reflection of light from freshly etched surfaces.[15] We estimate that the crystal orientation was accurate to ± 2°.

Most of the samples were irradiated with electrons of ~1.5 MeV, but in some cases electrons of ~5 and 45 MeV were also used. The irradiation conditions were always such as to keep the temperature rise in the sample to less than ~25 °C above room temperature.

In order to observe the defect absorption bands, the samples had to be cooled to temperatures be-

low ~180 °K, and most of the measurements reported here were made with the sample at 78 °K in a cryostat to be described below. The ir spectrometer used in the measurements was a Perkin-Elmer model 621 which is capable of covering the wavelength range 2.5–50 μ. The spectrometer was equipped with a wire-grid polarizer placed at the entrance slit to the monochromator. The isochronal annealing experiments were carried out in air in a temperature-controlled furnace (±1 °C). After each heat treatment the samples were thoroughly cleaned and lapped to eliminate the effects of oxide impurities at the surface.

A detailed description of the cryostat used has been given elsewhere.[16] Here we shall describe the general features of the cryostat and several important modifications made since its original use. Basically we used an Andonian Associates liquid-helium cryostat model MHD-3L-30N including the Andonian Associates option-24 tail piece. The cryostat and sample holder were constructed so that the stress could be applied to the sample while it was in the cryostat. The sample-stressing apparatus consisted of a $\frac{1}{4}$-in. diam rod concentric with a tube of 0.040-in. wall and $\frac{3}{4}$-in. o.d. constructed so as not to exert any forces on the cryostat. Three concentric shims along the length of the rod served to center it in the tube. All materials were either type-321 or -304 stainless steel. A 2-ton capacity hydraulic jack with a $\frac{3}{4}$-in. diam piston (having 1-in. maximum travel) was used to exert a force between the $\frac{1}{4}$-in.-diam rod and the outer $\frac{3}{4}$-in.-diam tube. The rod in turn transmitted the force to a solid stainless-steel plunger that had a smooth-sliding fit inside the hollow tube directly above the sample. To ensure uniform stress to the sample, and to prevent fracture, a 0.015-in. sheet of copper and a thin sheet of cardboard were placed between each end of the sample and the flat bearing surfaces of the piston and the plug at the end of the tube.

Our stress cryostat apparatus necessitated the use of cold windows which were exposed to either liquid-nitrogen or liquid-helium coolant. Our technique for making the vacuum-tight low-temperature seal of the windows involved use of silver chloride (AgCl) having dimensions 19×8×2.5 mm sealed with an epoxy[17] to a flexible copper housing ~0.015 in. thick. The copper housing was machined from a single piece of material 0.120 in. thick at the mounting flange. The copper flange was bolted to the cryostat tail piece with the vacuum seal made using indium gaskets. Windows constructed in this fashion were found to be capable of withstanding many thermal cycles (~100) before leaks developed.

III. EXPERIMENTAL RESULTS AND DISCUSSION

A. Production and Annealing in P- and As-doped Si

In Fig. 1 we give representative ir spectra for a phosphorus- and an arsenic-doped Si sample measured after irradiation with 1.5-MeV electrons to a fluence of 10^{18} e^-/cm^2. The results given in Fig. 1 are for samples originally doped to ~10^{17} atoms of P or As per cm^3. In phosphorus-doped material the dominant band is at 1150 cm^{-1}, with associated weaker bands at 1310, 970, 1000, 1040, 1450, and 1025 cm^{-1}. In arsenic-doped material

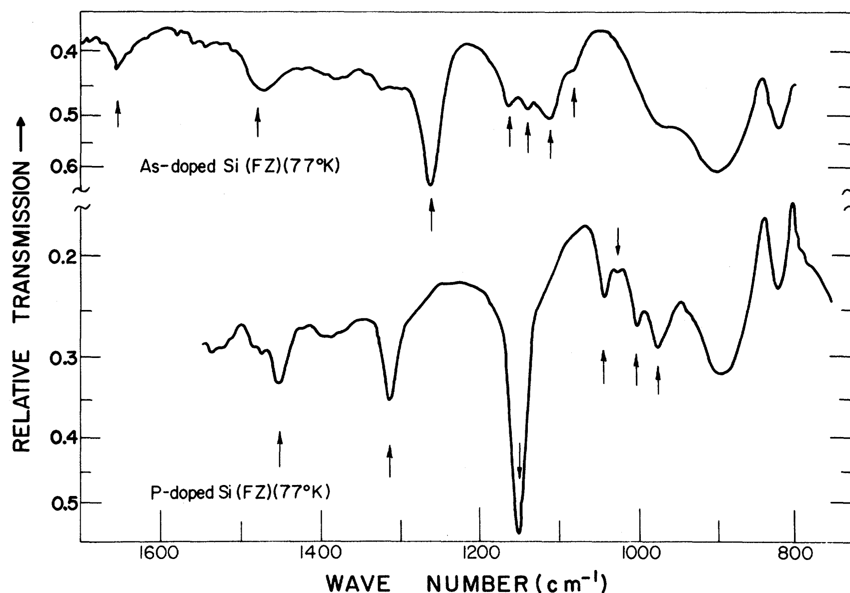

FIG. 1. ir spectra in the 800- to 1600-cm^{-1} wave-number range for a P- and an As-doped silicon sample (FZ: float-zone refined) after irradiation by 1.5-MeV electrons (~325 °K) to a fluence of 10^{18} e^-/cm^2. The measurements were made at 77 °K and the arrows indicate positions of radiation-produced bands.

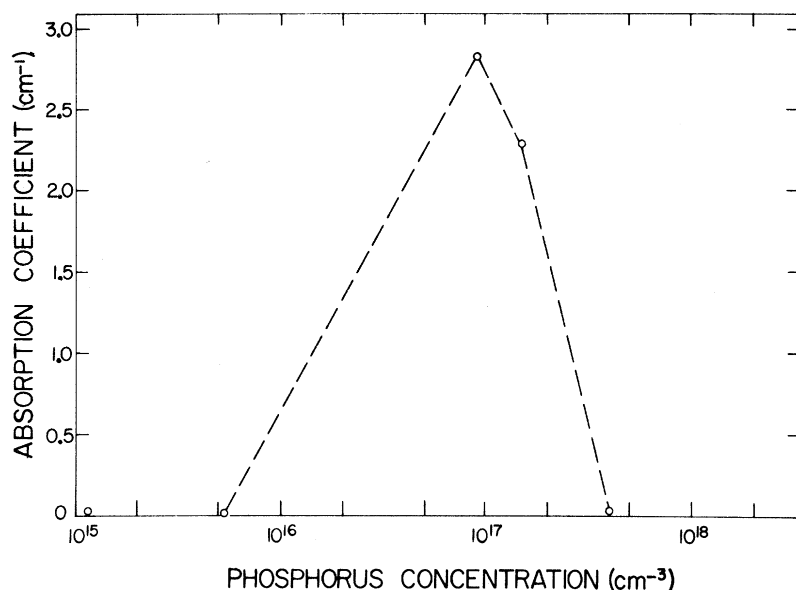

FIG. 2. Dependence of the absorption band at 1150 cm^{-1} in P-doped Si on the initial phosphorus concentration. In all measurements the 1.5-MeV electron fluence on the sample was adjusted so as to give maximum absorption.

the dominant band is at 1260 cm^{-1}, with weaker bands at 1480, 1080, 1110, 1135, 1160, and 1650 cm^{-1}. Similar bands were not observed in antimony-doped silicon ($\sim 10^{17}$-cm^{-3} Sb).

For the P-doped material, a study of the spectrum was made at 100, 87, 78, 65, and 7 °K. The relative amplitudes of the absorption peaks were found to be independent of temperature. The lines sharpen as the temperature is lowered but no significant sharpening of the peaks was observed below ~65 °K.

One rather striking property of the bands in P-doped material is that one apparently observes them only if the sample contains $10^{16}-10^{17}$ phosphorus atoms/cm^3. In Fig. 2 we give the dependence of the maximum intensity of the dominant 1150-cm^{-1} band on the phosphorus impurity concentration. Each of the experimental points shown in Fig. 2 are based on several irradiation experiments in which the fluence was varied to give maximum absorption at each impurity concentration. To date we have not yet made similar measurements on arsenic-doped material.

In Fig. 3, we plot the growth of the dominant absorption bands (1150 cm^{-1} in P-doped and 1260 cm^{-1} in As-doped silicon) vs fluence of 1.5-MeV electrons. We also show the uncompensated donor-electron concentration vs fluence as monitored by

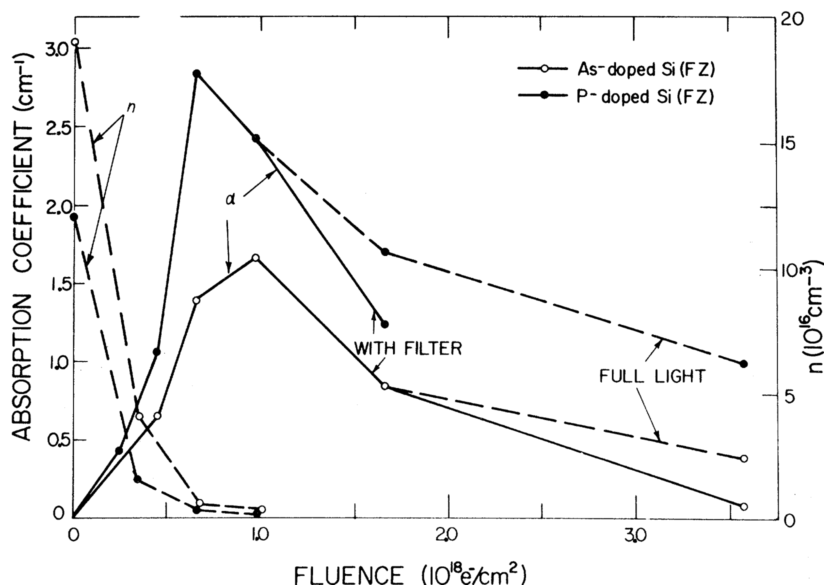

FIG. 3. Carrier concentration and absorption coefficient (1260-cm^{-1} band in As-doped and 1150-cm^{-1} band in P-doped Si) as a function of 1.5-MeV electron fluence. The carrier concentration was measured at 300 °K and the ir absorption measured at 78 °K.

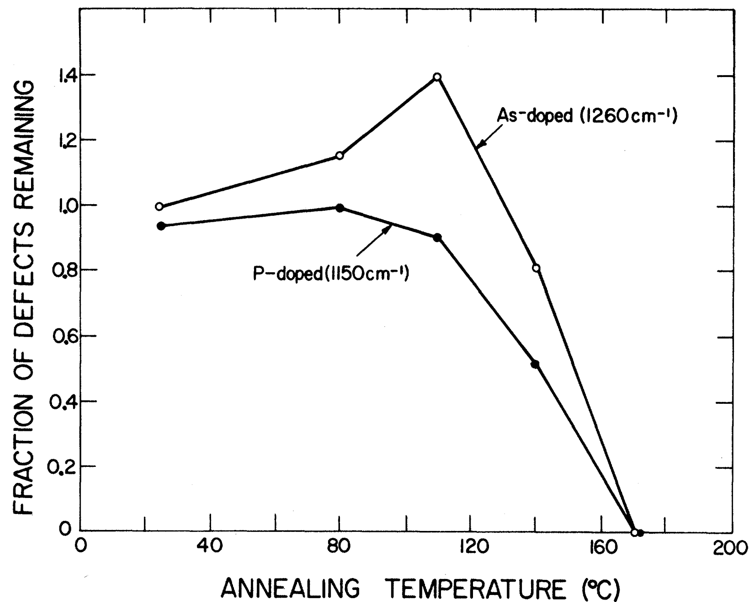

FIG. 4. Isochronal anneal (15 min at each temperature) of the dominant bands in P- and As-doped silicon.

the room-temperature resistivity. The growth of the bands is observed to increase as long as uncompensated donors remain. After the donor electrons are exhausted, the intensity of the bands saturates and then decreases with further dose. At higher doses, the band intensities are observed to increase when one allows the full light beam (i.e., all energies) to strike the sample as opposed to using a filter which cuts out light $< 3\mu$. This behavior reveals that the defects are still present at these higher doses but not in the correct charge state for observation. The higher-energy light presumably serves to create conduction electrons which can be trapped metastably at the defect to produce the bands. At all fluence levels, the relative amplitudes of all of the bands in each spectrum appears constant, each line displaying the same intensity vs fluence as the dominant one shown in the figure.

Isochronal annealing experiments (15 min at each temperature) were run on P- and As-doped Si ($\sim 10^{17}$ cm^{-3}) after irradiation with ~45-MeV electrons to a fluence of 2.1×10^{17} e^-/cm^2. The annealing results are given in Fig. 4. For both impurity types we observe one dominant annealing stage centered at 140–150 °C. Although the annealing results are only shown for the dominant bands in Fig. 4, the recovery of all the other bands (see Fig. 1) is identical to that given in Fig. 4.

B. Compressive-Stress Results in P-doped Si

The major portion of the experimental effort in this research was spent in detailed studies of the response of the radiation-induced bands to a uniaxial compressive stress. In our experiments we could vary the stress in a controlled manner with good monitoring of the pressure that was being exerted on the sample at all times. In our usual runs

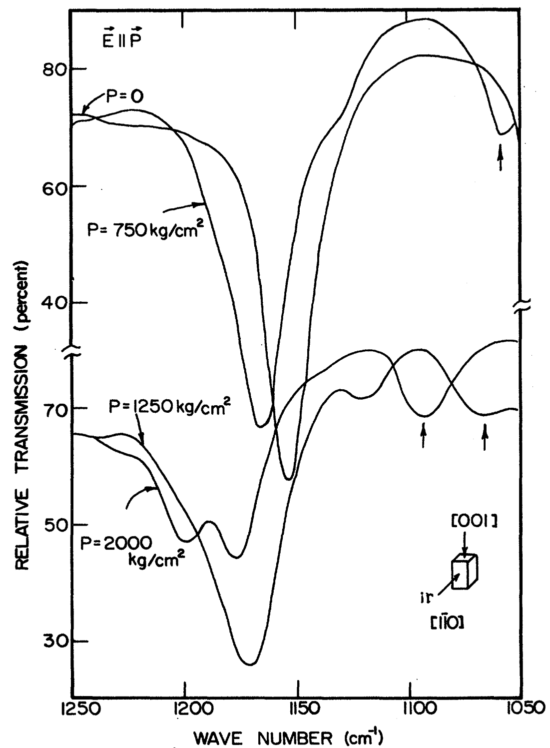

FIG. 5. Typical experimental curves showing the response of the 1150-cm^{-1} band in P-doped Si to compressive stress $\vec{P}$ in the [001] direction with $\vec{E} \parallel \vec{P}$ at 78 °K. The curves are shown for four different stress values at $\vec{P} = 0$, 750, 1250, and 2000 kg/cm^2.

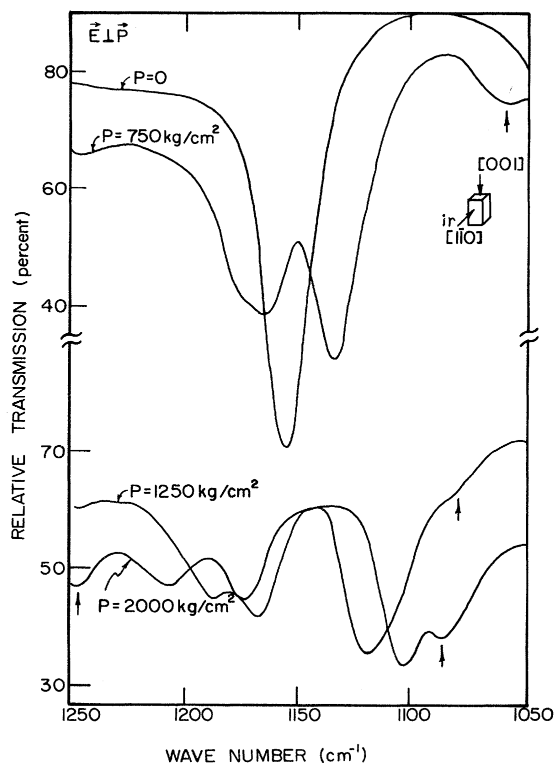

FIG. 6. Typical experimental curves showing the response of the 1150-cm^{-1} band in P-doped Si to compressive stress in the [001] direction with $\vec{E} \perp \vec{P}$ at 78 °K. The curves are shown for four different stress values at $\vec{P}$=0, 750, 1250, and 2000 kg/cm^2.

we first measured the spectrum without stress. Subsequent spectra were measured at successively higher stress, taken first with the light polarizer set to analyze light with the electric field vector $\vec{E}$ parallel to the axis of stress (denoted $E_{\parallel}$), and then the wavelength region of interest was scanned with $\vec{E}$ perpendicular to the axis of stress ($E_{\perp}$). The stress axis was always parallel to the long dimension of the sample. In Figs. 5 and 6 we show some typical results on the response of the 1150-cm^{-1} phosphorus-doped sample to a stress in the [001] direction with $\vec{E}$ parallel and perpendicular to the stress direction, respectively. In Fig. 5 we see that the band shifts to the high-wave-number side, broadens upon increase of stress, and then splits into two equal intensity components when stress reaches 2000 kg/cm^2. The band denoted by the arrow on the low-wave-number side of the spectra is a component of the 1040-cm^{-1} band which also shifts from the low- to the high-wave-number side with increase of stress. The results given in Fig. 6 show how the 1150-cm^{-1} band splits into two equal-intensity components at $\vec{P}$ = 750 kg/cm^2, and then the higher-energy component again splits into another pair of two equal-intensity components with the lower-energy component moving toward the low-wave-number side upon further increase of stress. The bands denoted by the arrows on the right-hand and left-hand sides of the figure are the components of the 1040- and 1310-cm^{-1} bands, respectively. Part of the reduction of transmission is due to the misalignment of the sample resulting from the application of the stress.

Although the bands at 1040, 1000, and 970 cm^{-1} are weak compared to the 1150-cm^{-1} band and although they are close together, one can still observe the general features of the splitting of the bands and their different response to polarized light if one examines closely the positions of the bands in the sequence of the stress spectra at different stresses. In Figs. 7 and 8, we present the typical response of the weaker-absorption bands in the 950- to 1080-cm^{-1} wave-number region for the P-doped sample under a [001] stress direction with $\vec{E} \parallel \vec{P}$ and $\vec{E} \perp \vec{P}$, respectively. Here again one can see that the 1040-cm^{-1} band splits into two components in which the higher-energy component is observed in both $E_{\parallel}$ (Fig. 7) and $E_{\perp}$ (Fig. 8) and the lower-energy component is only observed in $E_{\perp}$ (Fig. 8). The 1000- and 970-cm^{-1} bands also split into two components in which the higher-energy component is observed in $E_{\perp}$ (Fig. 8) and lower-

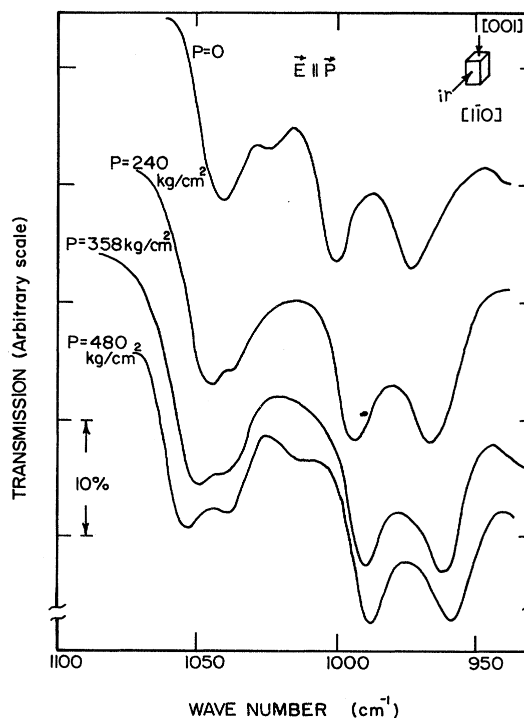

FIG. 7. Experimental curves showing the stress response of the weaker bands in the 950- to 1080-cm^{-1} wave-number region of P-doped Si to a [001] compressive stress with $\vec{E} \parallel \vec{P}$ at 78 °K. The curves are shown for four different stress values at $\vec{P}$=0, 240, 358, and 480 kg/cm^2.

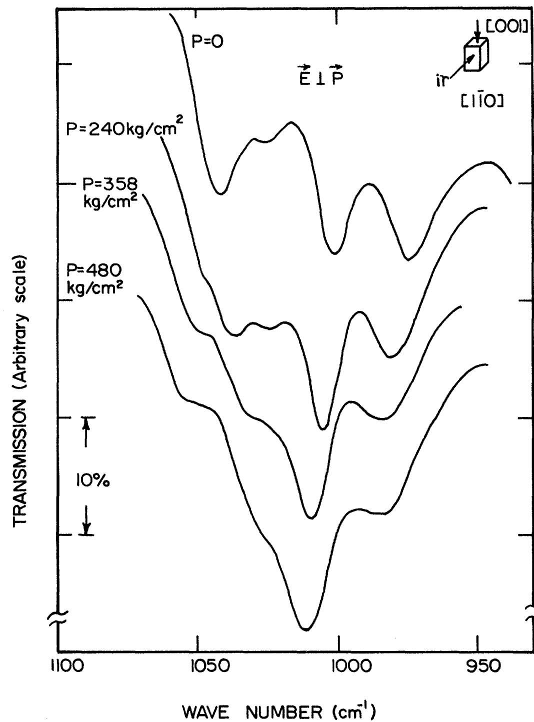

FIG. 8. Experimental curves showing the stress response of the weaker bands in the 950- to 1080-cm^{-1} wave-number region of P-doped Si to a [001] compressive stress with $\vec{E} \perp \vec{P}$ at 78 °K. The curves are shown for four different stress values at $\vec{P}=0$, 240, 358, and 480 kg/cm^2.

energy component is observed in $E_{\parallel}$ only (Fig. 7). For runs on the weaker bands, such as shown in Figs. 7 and 8, it was found convenient to place an intrinsic Si sample in the reference beam of the double-beam ir spectrometer and to use maximum gain and long integration times.

In Figs. 9–12 we have summarized the results of compressive stress on the bands at 970, 1000, 1040, 1150, and 1310 cm^{-1} in the P-doped sample. The direction of the incident light and the stress axis is shown on each figure. The experimental points ○, ×, and ● are the data points observed in perpendicular ($E_{\perp}$), parallel ($E_{\parallel}$), and both perpendicular and parallel, respectively. The solid lines, (⊥, ∥), and the numbers in the bracket are theoretical predictions of the split components, polarization property, and the ratio of relative intensity between the lines, which will be described in Sec. IV B. We were not able to obtain clear stress data on the 1450-cm^{-1} band because of the interference effects of water-vapor-absorption bands which could not be completely eliminated. Similarly, the weak band at 1025 cm^{-1} is so weak that is could not be studied.

In Fig. 13(b), we show schematically the experimentally estimated intensities of each of the components split out from the 1150 cm^{-1} band for each polarization of light.

Although the lines broaden with stress, the integrated area of each of the split out components appears to remain constant vs stress, within the accuracy of measurement. We conclude, therefore, that there is no dichroism associated with defect alignment in the stress field. In addition, no dichroism was observed in an experiment in which the sample was stressed at 100 °C and then cooled down to 78 °K with stress on.

In an additional experiment we made a careful search for photoconductivity associated with bands in the 900–140-cm^{-1} range of frequencies. The result was that no photoconductivity was observed.

Stress splittings were also studied in the arsenic-doped samples. Here, because of the weaker intensities of the spectrum, fewer lines could be studied in detail. The general features, however, match closely those seen for the phosphorus-doped sample.

C. General Conclusions

The fact that the relative intensities of the bands in each of the As- and P-doped samples are constant vs dose, vs anneal, and vs samples of different origin and different group-V atom concentration leads us to conclude that the bands are all associated with a single defect in each sample material. The band positions are different in the two materials. However, the similarity in the number of lines and their relative spacings and intensities allows us to conclude that the defect in both materials is basically the same defect but that the group-V atom is directly involved.

The dependence upon Fermi level, Fig. 3, reveals that the defect needs to trap an electron to give rise to the spectrum. From this, we conclude that we are dealing with an *electronic*-excitation spectrum (i.e., not *vibrational*, which, of course, also is often found in this spectral region). The temperature independence of the relative intensities of the lines reveals that the structure must arise from a manifold of *excited* states to which transitions can be made. (If some of the structure were associated with splittings in the ground state, the amplitudes would be temperature dependent, reflecting a Boltzmann population distribution between the levels). The same kind of argument allows us to conclude that the splittings observed under stress cannot be due to splittings of a degenerate ground state, or dichroism would again result.

To summarize, we are dealing with a defect complex which involves at least one group-V atom directly. The bands are the result of electronic excitation from an orbital singlet ground state to a manifold of excited states. In Secs. IV and V we

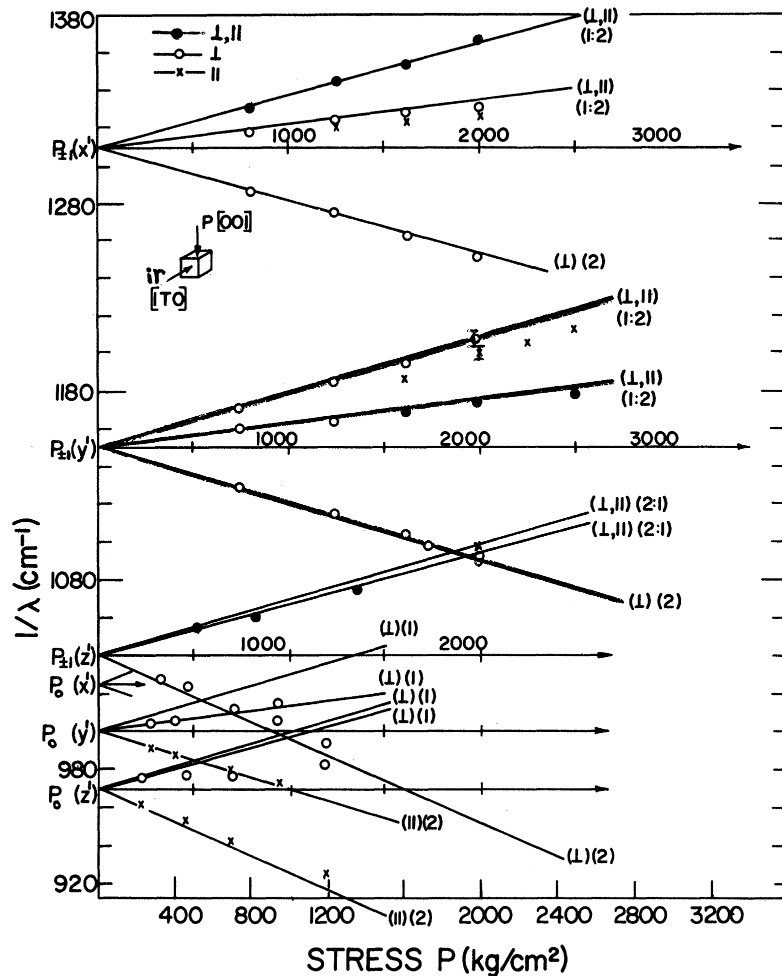

FIG. 9. The splitting of the 1310-, 1150-, 1040-, 1000-, and 970-cm^{-1} bands in P-doped Si at 78 °K, for $\vec{P} \parallel [001]$. The points are experimentally determined. The solid lines result from fitting to theory, see Sec. IV.

will consider what additional information the stress experiments can give about the nature of the defect.

IV. ANALYSIS OF STRESS SPLITTINGS

A. Group-Theoretical Classification

On general symmetry grounds, Kaplyanskii[12] has classified the behavior of optical transitions associated with centers of cubic symmetry under external stress. In addition, he has considered all possible types of noncubic centers in cubic crystals and classified the behavior of optical transitions between nondegenerate levels associated with those "orientationally degenerate" defects under stress.[13] Runciman[14] has extended this treatment to include the remaining four classes of spectra where both orientational and nonaccidental electronic degeneracy exist.

Superficially, therefore, one might be led to conclude that optical transitions associated with a defect in a cubic crystal must fall into one of these classes. We find, however, that it is not possible to fit our data satisfactorily to any of the classes. The number of split-out lines and their polarization properties cannot be fit. Let us therefore reconsider the assumptions inherent in this type of group-theoretical classification and see if we can understand its failure here.

One possible reason for failure has been previously suggested by Stoneham and Lanoo.[18] They considered the case of a Jahn-Teller distorted defect in which the distortion symmetry of the ground and excited states is different. As shown by these authors, this could apply only to a zero-phonon line of a therefore rather weak Jahn-Teller system. Since our spectrum has many lines and no evidence of phonon-assisted broad bands at higher energies, we argue that this cannot apply to our case.

Another possibility, to our knowledge not previously pointed out, is when *accidental* degeneracy exists. Symmetry arguments as to the number of lines and polarization, etc., then clearly can be wrong. In Sec. IV B, we consider the case in which

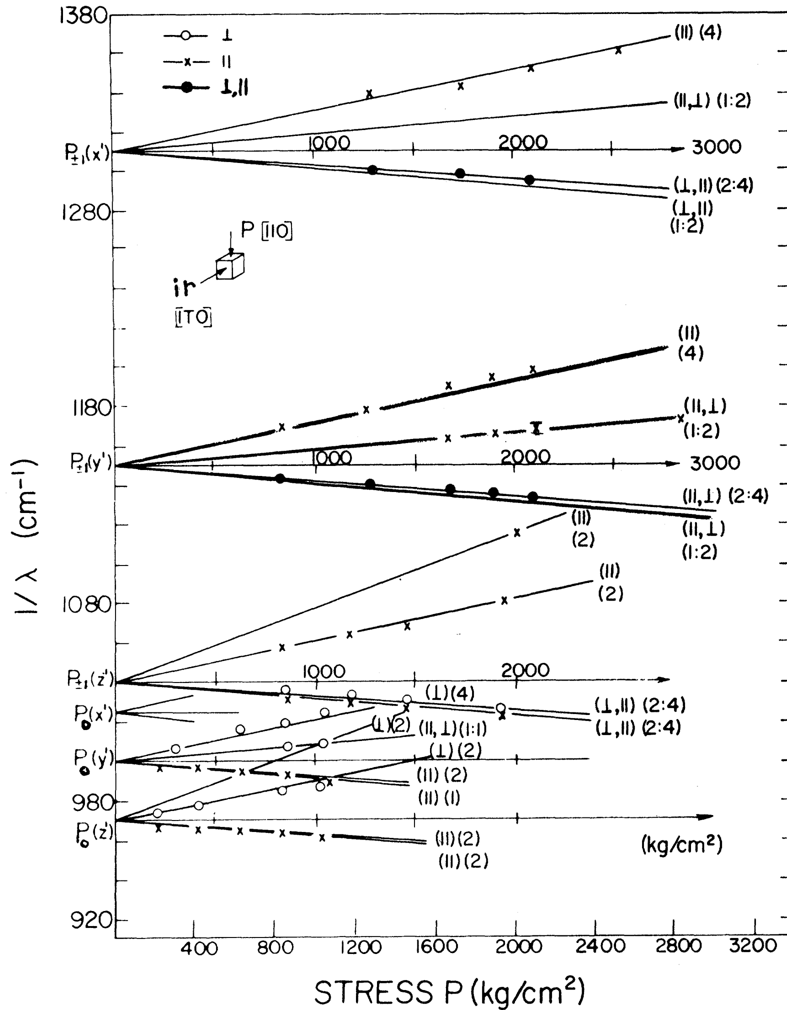

FIG. 10. The splitting of the 1310–, 1150–, 1040–, 1000–, and 970-cm^{-1} bands in P-doped Si at 78 °K. The stress in the [110] direction and light is incident in the [1̄10] direction; ⊥ and ∥ refer to polarization of $\vec{E}$ relative to $\vec{P}$. The points are experimentally determined. The solid lines represent fit to theory, Sec. IV.

the excited states are shallow effective-mass-like states made up from the multivalleyed-conduction-band minima of silicon. We will see that this automatically provides accidental degeneracy in these excited states, which can explain our observed results.

B. Theory of Shallow Effective-Mass Donor States

For an electron attracted Coulombically to a positively charged core in an insulating solid, an infinite ladder of excited states exist. In silicon, Kohn and Luttinger[19,20] have shown that for the states close to the conduction-band edge ($\lesssim 0.03$ eV from the band edge) the wave function can be approximated by

$$\Psi(\vec{r}) = \sum_{j=1}^{6} \alpha_j F_j(\vec{r})\, \phi_j(\vec{r}) . \qquad (1)$$

Here $\phi_j(\vec{r})$ is the Bloch wave for the jth minimum of the conduction band, α_j are numerical coefficients, and the sum is over the six equivalent $\langle 100\rangle$ conduction-band minima (valleys). $F_j(\vec{r})$ is an envelope function which, for the jth valley on the z axis, satisfies the equation

$$\left[-\frac{\hbar^2}{2m_l}\frac{\partial^2}{\partial z^2} - \frac{\hbar^2}{2m_t}\left(\frac{\partial^2}{\partial x^2} + \frac{\partial^2}{\partial y^2}\right) + \frac{1}{\kappa} V(\vec{r})\right] F_z(\vec{r}) = E F_z(\vec{r}) . \qquad (2)$$

Here m_l and m_t are the longitudinal and transverse effective masses for an electron at the conduction-band minimum, κ is the static dielectric constant, $V(\vec{r})$ is the potential associated with the attractive core, and E is the energy of the donor state relative to the conduction-band minimum.

If the core is a simple point charge, $+Ze$, the potential becomes

$$V(\vec{r}) \cong -Ze^2/r \qquad (3)$$

and the functions $F_j(\vec{r})$ are simple "hydrogeniclike" envelope functions. In our case, we will be led to

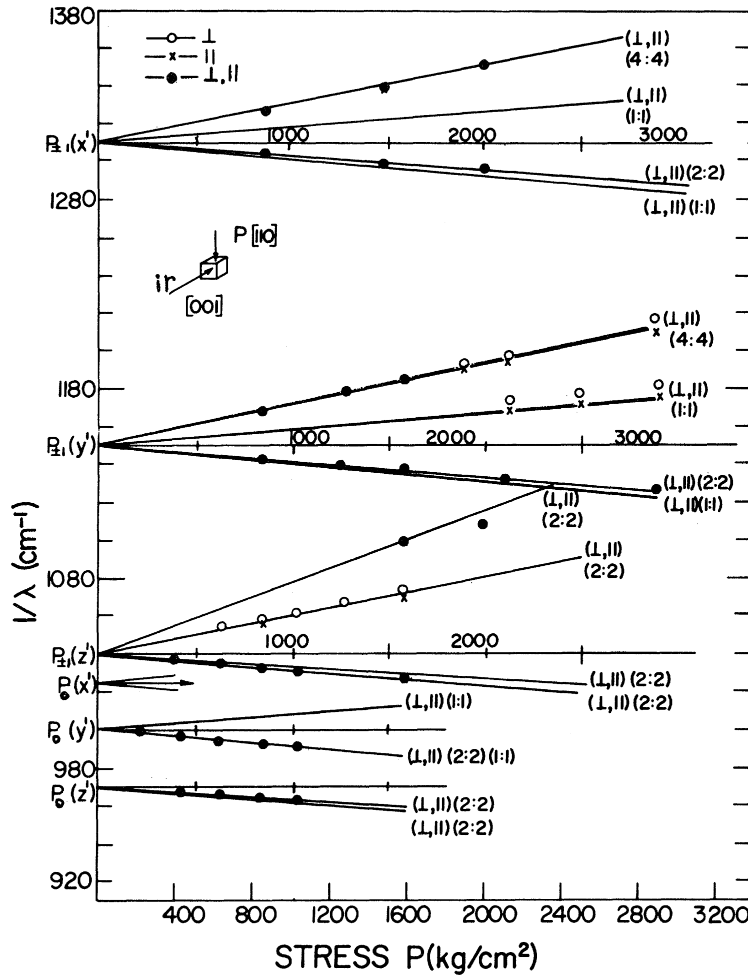

FIG. 11. The splitting of the 1310-, 1150-, 1040-, 1000-, and 970-cm^{-1} bands in P-doped Si at 78 °K. The stress $\vec{P}$ is in the [110] direction and light is incident in the [001] direction; ⊥ and ∥ refer to polarization of $\vec{E}$ relative to $\vec{P}$. The points are experimentally determined. The solid lines represent fit to theory, Sec. IV.

conclude in subsequent sections that the core is anisotropic. However, for large-orbit shallow excited states, we anticipate that the monopole term dominates and that Eq. (3) represents, therefore, a good starting point. The anisotropy of the core can then be treated as a perturbation.

1. T_d Symmetry

For a single point charge on a substitutional (or interstitial) lattice site, the point group symmetry is T_d. This is the situation that prevails for the simple substitutional (P, As, Sb, Bi, Mg) and interstitial (Li) donors. Solution of Eqs. (2) and (3) for this case[19–21] leads to a ladder of hydrogenic states $1S$, $2S$, $2P_0$, $2P_{\pm 1}$, $3S$, $3P_0$, $3P_{\pm 1}$, etc., whose energy-level positions have been verified in considerable detail by comparison to optical excitation spectra.[22,23] (The splitting of the P states arises from the anisotropy of the effective mass. P_0 is the state with $M=0$, and $P_{\pm 1}$ is the state with $M=\pm 1$, where the quantization axis is the axis of the displaced conduction-band minimum.)

"Central-cell" corrections are found to be important only for the ground $1S$ manifold. Here the sixfold degeneracy arising from the six conduction-band minima is partially lifted giving a singlet A_1, doublet E, and triplet T_2. The excited P states retain this additional sixfold degeneracy, which from symmetry considerations must be considered "accidental" degeneracy. This is illustrated in Fig. 14(a) where the sixfold degeneracy of the $2P_0$ state is made up of accidentally degenerate $A_1 + E + T_2$ states in T_d, etc. (The ordering of the $1S$ states is not determined by symmetry. The order shown in the figure is that found experimentally for the substitutional donor.)

The intensity of an optical-absorption transition between two of the states is proportional to the square of the momentum matrix element between them. This leads to[20]

$$|\langle 1|P_\alpha|2\rangle|^2 \sim \left(\sum_{j=1}^{N} \alpha_j^{(1)*}\,\alpha_j^{(2)}\,(F_j^{(1)},\ x_\alpha F_j^{(2)})\right)^2 . \tag{4}$$

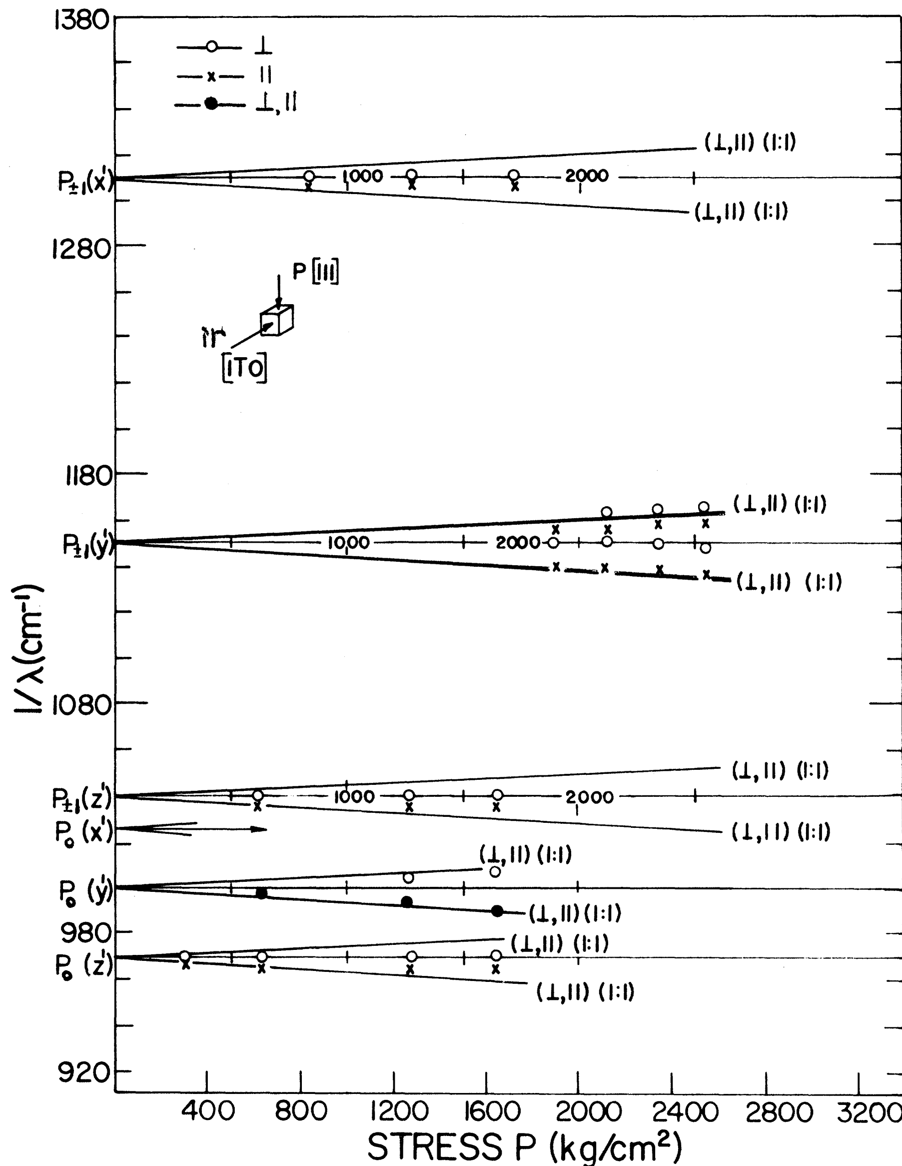

FIG. 12. The splitting of the 1310-, 1150-, 1040-, 1000-, and 970-cm^{-1} bands in P-doped Si at 78 °K. The stress $\vec{P}$ is in the [111] direction and light is incident in the [$1\bar{1}0$] direction; ⊥ and ∥ refer to polarization of $\vec{E}$ relative to $\vec{P}$. The points are experimentally determined. The solid lines represent fit to theory, Sec. IV.

The polarization properties and selection rules, therefore, reflect the dipole-moment matrix elements between the hydrogenic modulating envelope functions $F_j^{(n)}$.

2. *Effect of Stress*

Stress produces strains which can shift the conduction-band minima with respect to one another and therefore remove some of the degeneracy associated with the multivalleyed character of the effective-mass states. The formalism for this has been developed by Herring[24] and Herring and Vogt[25] in terms of the "dilatation" Ξ_d and "uniaxial" Ξ_u deformation potentials. Uniform dilatation arising from the hydrostatic component of stress, shifts all valleys equally and is not of concern to us. The coupling to the nonhydrostatic components leads, in silicon, to a simple expression for the shift of the jth valley

$$\Delta E^{(j)} = \tfrac{1}{3}\,\Xi_u (S_{11} - S_{12}) \sum_i (3\delta_{ij} - 1)\,\sigma_{ii}\,. \qquad (5)$$

Here S_{11}, S_{12} are the elastic moduli of silicon, σ_{ii} are the diagonal components of the stress tensor,[26] and the sum is over the three cubic axes (i) of silicon.

The effect of stress on the states given by Eq. (1) is therefore to split out those functions made up from each of the differently directed conduction-band minima.[23] This is illustrated in Fig. 14(b) for[26] $\sigma_{xx} > \sigma_{yy} > \sigma_{zz}$.

In order to keep track of the states and the optical selection rules, we find it convenient to use

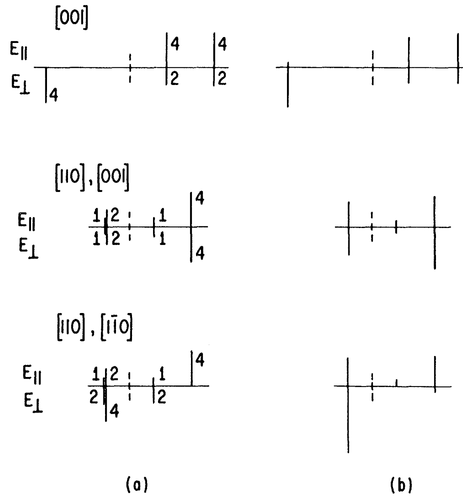

FIG. 13. Comparison of predicted and observed intensities of components split from 1150-cm^{-1} line in P-doped material under [001] and [110] compressional stress: (a) predicted for monoclinic-II center for transition to $2P_{\pm}(y')$ excited state; (b) estimated intensities from experiment. For [110] stress, the second direction quoted is the viewing direction (i.e., direction of light propagation). $E_{\parallel}$ refers to light polarized with $\vec{E}$ parallel to the stress and $E_{\perp}$ with $\vec{E}$ perpendicular to the stress.

the following labeling scheme: For the $2P$ states, each F_j has three solutions, which we label X_j, Y_j, or Z_j, corresponding to the three similarly directed P functions. In this notation, the $2P_0$ and $2P_{\pm1}$ states are made up from linear combinations of

$$2P_0 \begin{cases} X_{\pm x}\ \phi_{\pm x} \\ Y_{\pm y}\ \phi_{\pm y} \\ Z_{\pm z}\ \phi_{\pm z} \end{cases}, \qquad 2P_{\pm1} \begin{cases} Y_{\pm x}\ \phi_{\pm x},\ Z_{\pm x}\ \phi_{\pm x} \\ X_{\pm y}\ \phi_{\pm y},\ Z_{\pm y}\ \phi_{\pm y} \\ X_{\pm z}\ \phi_{\pm z},\ Y_{\pm z}\ \phi_{\pm z} \end{cases}. \qquad (6)$$

Here, for instance, the function $Y_{+x}\phi_{+x}$ denotes the product of the Bloch state associated with the conduction-band minimum in the $+x$ direction and the corresponding modulating P_{+x} function envelope that is oriented along the Y axis (and is therefore made up from $M=\pm1$ states).

In the effective-mass treatment, stress couples only to the $\phi_{\pm j}$ part of the wave function [Eq. (5)] allowing one to immediately identify the split out states as shown in Fig. 14(b). The optical selection rules, on the other hand [Eq. (4)], reflect the modulating part of the wave function (X_j, etc.), and the corresponding optical selection rules are also indicated in the figure.

Stress splittings of the excited effective-mass states for a variety of substitutional and interstitial donors have been reported and the general features of Fig. 14(b) and Eqs. (4) and (5) have been confirmed in detail.[23,27–30] Although these authors have not made this observation, it is interesting to point out that the polarizations and splittings for the T_d effective-mass donor described here do not fit Kaplyanskii's group-theoretical classification. The results cannot be fit by his tables for a defect with T_d symmetry.[12] The reason for this failure stems directly from the *accidental degeneracy* inherent in the problem. The $2P_0$ state is actually made up by symmetry of A, E, and T_2 states, which are degenerate by accident. Kaplyanskii's tables apply only to first-order splittings of each of the states separately. The accidental degeneracy allows stress mixing of the states and his analysis is inappropriate. The same arguments apply for the accidental degeneracy of the twelve states $(2T_1+2T_2)$ of $2P_{\pm1}$.

3. *Donor with Anisotropic Core*

If the donor defect has an anisotropic core, i.e., if the symmetry is not T_d, the ground $1S$ states may be severely altered. However, the large-orbit excited states can be expected to maintain their general character and, as a first approximation, be simply split as if by the strain field of the anisotropic core. Because the effective-mass excited states

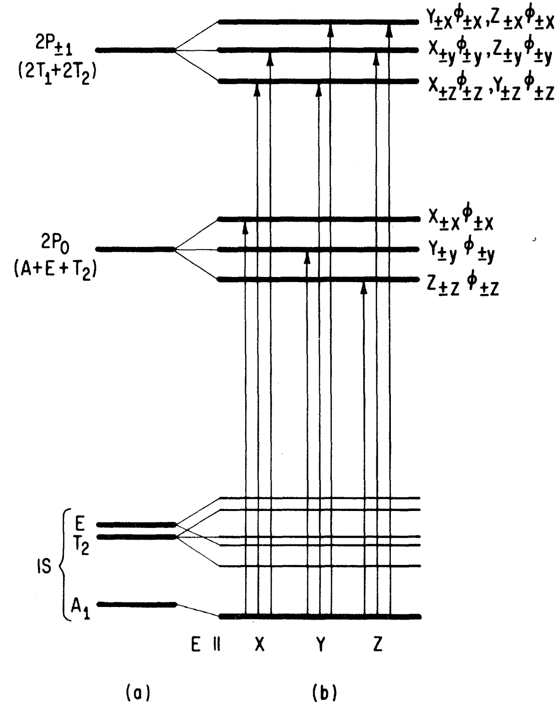

FIG. 14. Effect of stress on the $1S$, $2P_0$, and $2P_{\pm1}$ effective-mass states for a shallow donor with T_d symmetry: (a) zero stress, (b) $\sigma_{xx} > \sigma_{yy} > \sigma_{zz}$. Allowed optical transitions and polarization selection rules from the ground state are shown.

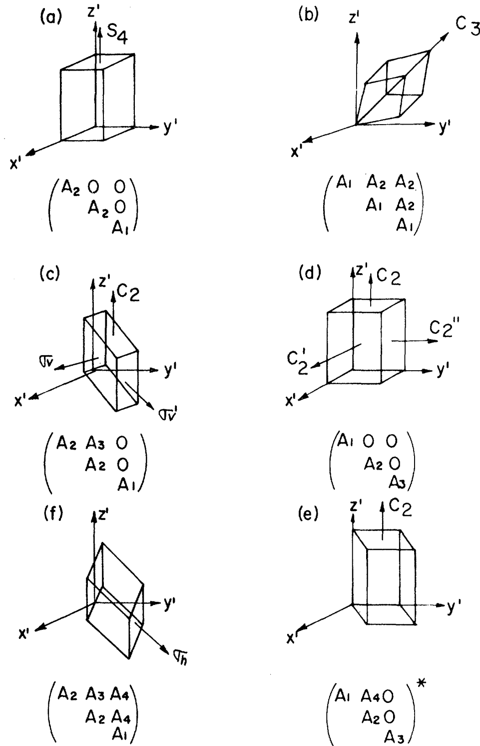

FIG. 15. Symmetry classification and form of the piezospectroscopic tensor for anisotropic centers in a cubic lattice. (After A. Kaplyanskii, Ref. 13. The labels for the tensor components of monoclinic II differ from that of Kaplyanskii; see Ref. 31). The x', y', z' axes are the cubic axes.

couple only to the diagonal components σ_{ii} of the strain tensor, the most general anisotropic core will still then tend to split each of the excited $2P_0$, $2P_{\pm1}$, etc., states into three, resulting from the different components σ_{xx}, σ_{yy}, and σ_{zz}, as shown in Fig. 14(b). Figure 14(b), therefore, serves as a convenient starting point for the problem of interest.

We see immediately that such a defect will display many absorption lines, consistent with the observation on our defects. In addition the separation between lines will reflect details of the core (i.e., the magnitude of the effective strain field), which is consistent with the observation of a similar number of lines but different spacing for the As and P centers. Let us therefore investigate the effect of external stress on such a center and see if this can be explained.

For convenience, we assume that the splittings of the $2P_0$, $2P_{\pm1}$, etc., states due to the anisotropic core are small enough that the linear coupling to strain given by Eq. (5) is still valid for all excited states. The excited states therefore still couple only to the diagonal components of strain. We allow the ground state, however, to couple to all components of strain, and for this we use directly the formalism of Kaplyanskii[13] for orientational degenerate centers. His formalism states that the energy of the state can be written as

$$\sum_{i,j} A_{ij}\sigma_{ij} , \tag{7}$$

where $\underline{A}$ is the *piezospectroscopic* tensor. The form of $\underline{A}$ and the number of independent coefficients A_{ij} depend upon the symmetry of the defect, which he has classified into seven symmetry types: tetragonal, trigonal, rhombic I, rhombic II, monoclinic I, monoclinic II, and triclinic. We show in Fig. 15 a summary of his classification.[31] The symmetry operations relevant to the diamond lattice (subgroups of T_d) are shown.

Under stress, the shift of an optical transition is then calculated as the difference between the shift of the excited state determined by Eq. (5) and the shift of the ground state given by Eq. (7). We assume, as before, that the optical selection rules are determined by the envelope function of the excited effective-mass state. The result for all symmetry classes of defects (excluding triclinic) are summarized in Table I. The rhombic I and tetragonal centers are special cases of monoclinic I (i.e., $A_4=0$ for rhombic; $A_4=A_3=0$ for tetragonal) and are therefore not included separately. Similarly, rhombic II is a special case of monoclinic II[31] (with $A_4=0$).

To demonstrate how these were calculated, we show in Fig. 16 the case for a monoclinic II center with compressive stress parallel to the [001] direction. The levels in panel (a) are those in the absence of stress. The wave functions identified in this panel for each state come directly from Fig. 14, with the exception that the axes are *primed* to denote that they now refer to the internal axes of the anisotropic defect core (see Fig. 15). We have also shortened the notation, with $Y(x)$ denoting $Y_{\pm x}\ \phi_{\pm x}$, etc. We reserve the unprimed axes for the macroscopic crystal, with respect to which stress will be applied, optical polarization measured, etc. There are, therefore, six distinguishable defect orientations corresponding to the 3! ways the primed defect-axis system can be placed in the unprimed crystal system. These are displayed in panels (b)–(g) where the corresponding wave functions are labeled in the macroscopic-crystal unprimed-axis system (obtained simply by permuting the X, Y, Z axes). The response to stress and the polarization selection rules shown now follow directly as before with the first term of the wave function (envelope) giving the selection rules and the second term (the conduction-band minimum) giving the stress response.

In Table I, the results are tabulated for all sym-

TABLE I. Energy shifts and polarization properties vs compressional stress of optical transitions to excited effective-mass states for anisotropic defects in silicon.

		$P \parallel [001]$			$P \parallel [111]$			$P \parallel [110]$		
Type of centers	Excited states (valley)	Energy shift	$P_{\pm 1}$ $I_\parallel : I_\perp$	P_0 $I_\parallel : I_\perp$	Energy shift	$P_{\pm 1}$ $I_\parallel : I_\perp$	P_0 $I_\parallel : I_\perp$	Energy shift	$P_{\pm 1}$ $I_{110} : I_{001} : I_{\bar{1}10}$	P_0 $I_{110} : I_{001} : I_{\bar{1}10}$
		$\epsilon + A_1$	4 : 2	0 : 4	$A_1 + 2A_2$	1 : 1	1 : 1	$\epsilon + A_1 + A_2$	1 : 0 : 1	0 : 2 : 0
Trigonal	$x' - y' - z'$	$-2\epsilon + A_1$	0 : 2	4 : 0	$A_1 - \frac{2}{3}A_2$	3 : 3	3 : 3	$\epsilon + A_1 - A_2$	1 : 0 : 1	0 : 2 : 0
								$-\frac{1}{2}\epsilon + A_1 + A_2$	1 : 2 : 1	2 : 0 : 2
								$-\frac{1}{2}\epsilon + A_1 - A_2$	1 : 2 : 1	2 : 0 : 2
		$\epsilon + A_1$	4 : 2	0 : 2	$\frac{1}{3}(A_1 + 2A_2 + 2A_3)$	4 : 4	4 : 4	$\epsilon + \frac{1}{2}(A_1 + A_2 + 2A_4)$	2 : 0 : 2	0 : 2 : 0
		$\epsilon + A_2$	4 : 2	0 : 2	$\frac{1}{3}(A_1 + 2A_2 - 2A_3 + 4A_4)$	2 : 2	2 : 2	$\epsilon + \frac{1}{2}(A_1 + A_2 - 2A_4)$	2 : 0 : 2	0 : 2 : 0
Monoclinic I	$x' - y'$	$-2\epsilon + A_2$	0 : 4	4 : 0	$\frac{1}{3}(A_1 + 2A_2 - 2A_3 - 4A_4)$	2 : 2	2 : 2	$-\frac{1}{2}\epsilon + A_2 + A_3$	1 : 2 : 1	1 : 0 : 1
(Rhombic I								$-\frac{1}{2}\epsilon + A_2 - A_3$	1 : 2 : 1	1 : 0 : 1
$A_4 = 0$)								$-\frac{1}{2}\epsilon + \frac{1}{2}(A_1 + A_2 + 2A_4)$	1 : 2 : 1	1 : 0 : 1
(Tetragonal								$-\frac{1}{2}\epsilon + \frac{1}{2}(A_1 + A_2 - 2A_4)$	1 : 2 : 1	1 : 0 : 1
$A_3 = A_4 = 0$)										
		$\epsilon + A_2$	4 : 2	0 : 4	$\frac{1}{3}(A_1 + 2A_2 + 2A_3)$	2 : 2	2 : 2	$\epsilon + A_2 + A_3$	1 : 0 : 1	0 : 2 : 0
	z'	$-2\epsilon + A_1$	0 : 2	4 : 0	$\frac{1}{3}(A_1 + 2A_2 - 2A_3 + 2A_4)$	1 : 1	1 : 1	$\epsilon + A_2 - A_3$	1 : 0 : 1	0 : 2 : 0
					$\frac{1}{3}(A_1 + 2A_2 - 2A_3 - 2A_4)$	1 : 1	1 : 1	$-\frac{1}{2}\epsilon + \frac{1}{2}(A_1 + A_2 + 2A_4)$	1 : 2 : 1	2 : 0 : 2
								$-\frac{1}{2}\epsilon + \frac{1}{2}(A_1 + A_2 - 2A_4)$	1 : 2 : 1	2 : 0 : 2
		$\epsilon + A_2$	4 : 2	0 : 2	$\frac{1}{3}(A_1 + A_2 + A_3 + 2A_4)$	4 : 4	2 : 2	$\epsilon + \frac{1}{2}(A_2 + A_3)$	4 : 0 : 4	0 : 4 : 0
	x'	$\epsilon + A_3$	4 : 2	0 : 2	$\frac{1}{3}(A_1 + A_2 + A_3 - 2A_4)$	4 : 4	2 : 2	$-\frac{1}{2}\epsilon + \frac{1}{2}(A_1 + A_3)$	2 : 4 : 2	2 : 0 : 2
		$-2\epsilon + A_1$	0 : 4	4 : 0				$-\frac{1}{2}\epsilon + \frac{1}{2}(A_1 + A_2 + 2A_4)$	1 : 2 : 1	1 : 0 : 1
								$-\frac{1}{2}\epsilon + \frac{1}{2}(A_1 + A_2 - 2A_4)$	1 : 2 : 1	1 : 0 : 1
Monoclinic II										
(Rhombic II		$\epsilon + A_1$	4 : 2	0 : 2	$\frac{1}{3}(A_1 + A_2 + A_3 + 2A_4)$	4 : 4	2 : 2	$\epsilon + \frac{1}{2}(A_1 + A_3)$	4 : 0 : 4	0 : 4 : 0
$A_4 = 0$)	y'	$\epsilon + A_3$	4 : 2	0 : 2	$\frac{1}{3}(A_1 + A_2 + A_3 - 2A_4)$	4 : 4	2 : 2	$-\frac{1}{2}\epsilon + \frac{1}{2}(A_2 + A_3)$	2 : 4 : 2	2 : 0 : 2
		$-2\epsilon + A_2$	0 : 4	4 : 0				$-\frac{1}{2}\epsilon + \frac{1}{2}(A_1 + A_2 + 2A_4)$	1 : 2 : 1	1 : 0 : 1
								$-\frac{1}{2}\epsilon + \frac{1}{2}(A_1 + A_2 - 2A_4)$	1 : 2 : 1	1 : 0 : 1
		$\epsilon + A_1$	4 : 2	0 : 2	$\frac{1}{3}(A_1 + A_2 + A_3 + 2A_4)$	4 : 4	2 : 2	$\epsilon + \frac{1}{2}(A_1 + A_2 + 2A_4)$	2 : 0 : 2	0 : 2 : 0
	z'	$\epsilon + A_2$	4 : 2	0 : 2	$\frac{1}{3}(A_1 + A_2 + A_3 - 2A_4)$	4 : 4	2 : 2	$\epsilon + \frac{1}{2}(A_1 + A_2 - 2A_4)$	2 : 0 : 2	0 : 2 : 0
		$-2\epsilon + A_3$	0 : 4	4 : 0				$-\frac{1}{2}\epsilon + \frac{1}{2}(A_1 + A_3)$	2 : 4 : 2	2 : 0 : 2
								$-\frac{1}{2}\epsilon + \frac{1}{2}(A_2 + A_3)$	2 : 4 : 2	2 : 0 : 2

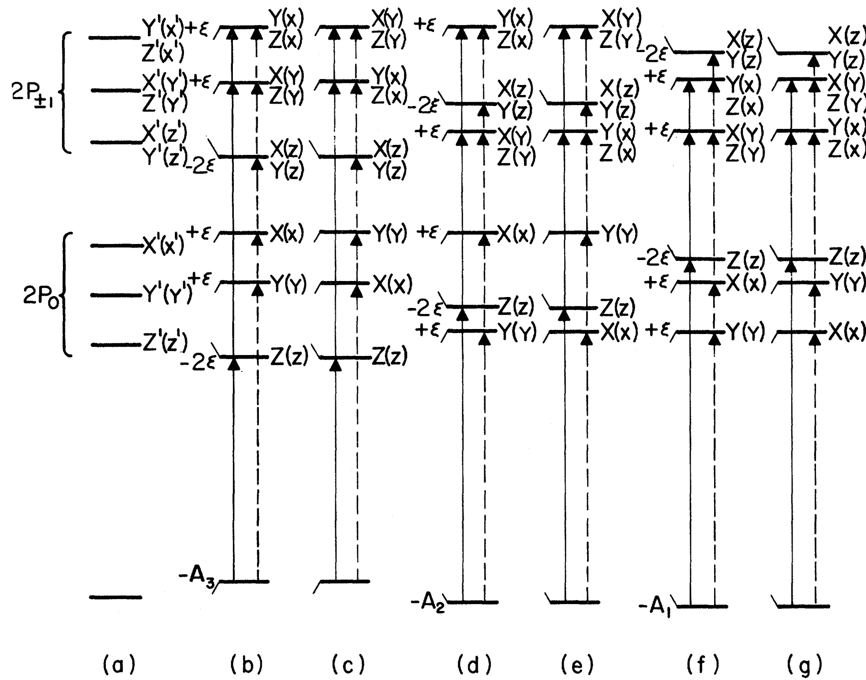

FIG. 16. Effect of compressional stress $\vec{P}\parallel[001]$ on a donor with an anisotropic core of monoclinic-II symmetry. (a) Zero stress. The primed axes refer to the defect axes as per Fig. 15. (b)–(g): The six differently oriented defects, under stress. The unprimed axes refer to the macroscopic crystal axes. The solid lines are the allowed optical transitions for $\vec{E}\parallel[001]$ and the dotted lines are for $\vec{E}\perp[001]$.

metry classes for unit *compressional* stress $\vec{P}$ along the three crystallographic directions [001], [111], and [110]. *Compression* was chosen because it conforms to the usual experimental condition. It also conforms to the convention of Table 3 of Kaplyanskii,[13] and our table, therefore, represents a direct extension of his orientational degeneracy classification to include the effect of the accidental degeneracy for the excited effective-mass states in silicon. In the table the splitting of the excited states per unit stress P is expressed, from Eq. (5), in terms of the single parameter

$$\epsilon = \tfrac{1}{3}\Xi_u\,(S_{11} - S_{12})\,. \tag{8}$$

The particular transition involved is identified by the "valley" associated with the corresponding excited state.

C. Analysis of Stress Splittings

For comparison with the experimental results, using Table I, we find our best fit to the data if we assume a center of monoclinic-II symmetry. The values of piezospectroscopic-tensor components $\underline{A}$ and ϵ determined by this fit are given in Table II, and the calculated splittings of the lines are plotted as the solid lines in Figs. 9–12, along with the predicted polarization properties. The transitions are identified in the figures by the corresponding excited state, with $P_{\pm1}(x')$ denoting the $P_{\pm1}$ state made up from the x' valleys, etc. (The choice of which axis is labeled x', y', or z' is not arbitrary but must conform to the convention of Fig. 15. The components of $\underline{A}$ given in Table II require the assignment as shown in Figs. 9–12.) The identification of the transitions as shown in Figs. 9–12 is determined by the stress spectra of the bands rather than by the relative intensities of the unstressed lines, since the ground-state wave functions are no longer symmetric due to the anisotropy of the core which has a monoclinic-II symmetry and the intensity of an optical-absorption transition between the ground and excited state is no longer expressable simply by Eq. (4). The band at 1150 cm^{-1} which is much stronger than other bands reveals that the ground-state wave functions have a large amplitude in the y' direction. A similar fit can also be made to the spectrum in the As-doped sample. The corresponding values for $\underline{A}$ and ϵ are also given in Table II for the As-doped samples.

As can be seen in Figs. 9–12, for all three stress directions, the number of components and the magnitude of the splittings can be satisfactorily accounted for. In addition, the predicted relative intensity and polarization of each component are for the most part in reasonable agreement (see Fig. 13).

The value of ϵ, from Eq. (7) gives $\Xi_u = 7.2 \pm 0.4$

TABLE II. Piezospectroscopic tensor components (10^{-3} cm^{-1}/kg cm^{-2}) for monoclinic-II symmetry core.

	A_1	A_2	A_3	A_4	ϵ
P doped	$+10\pm0.5$	$+9\pm0.5$	-6 ± 0.3	$+8.5\pm0.4$	19 ± 1
As doped	$+6.5\pm0.3$	$+5.5\pm0.3$	-8 ± 0.4	$+5\pm0.3$	19 ± 1

eV. This is in very good agreement with the value 7.9 ± 0.2 eV determined directly by stress splitting of the shallow-tetrahedral-donor spectra.[29,32] This, plus the fact that a single value of ϵ suffices for all components of both the phosphorus- and arsenic-associated spectra leads us to conclude that our basic model is correct–that the spectrum arises from transitions to excited large-orbit effective-mass-like states.

The core clearly has low symmetry. Our best fit is with monoclinic II. But it is not perfect. In Fig. 13, we show a comparison of the predicted intensity in each polarization vs the experimentally estimated values for the 1150-cm^{-1} line of the phosphorus-doped sample. This is the only line intense enough for such a comparison. We note that one component for $\vec{P} \parallel [110]$ is predicted to be seen for all polarizations but was not observed experimentally for $\vec{E} \parallel [001]$. Otherwise the agreement is very good.

It is possible that the component is actually present but has been missed experimentally. The lines broaden with applied stress and extracting the component from the background is difficult. It must be kept in mind, however, that detailed agreement should not be expected anyway. We have made certain simplifying assumptions in deriving Table I that are not valid in detail. In particular, we have treated the effect of the core as a small perturbation upon the T_d donor states. The observed splittings, on the other hand, are not actually small with respect to the original spacings in T_d and, as a result, admixtures between the $1S$, $2P_0$, $2P_{\pm1}$, and higher states undoubtedly occur. Similarly, intervalley coupling may be important. In the absence of these interactions, the transition dipole moment will coincide, as we have assumed, with the x', y', z' axes of the defect (the excited state composed of modulating function X couples to the ground state only through the dipole matrix elements of X, etc.), and this has led to the selection rules and intensities shown in the table.

In view of this, we accept the over-all agreement as satisfactory. We conclude that the model of an anisotropic defect with transitions to large-orbit effective-mass states does serve to explain the essential features of the experimental results. The symmetry of the core and the coupling of its ground state to the stress field as given by $\underline{A}$ indicate a defect of low symmetry. Monoclinic II gives a satisfactory fit but the symmetry could be lower (triclinic).

V. SUMMARY AND DISCUSSION

A series of sharp ir-absorption bands are produced by high-energy electron irradiation in phosphorus- and arsenic-doped float-zone-refined silicon. The band positions and spacings are different in the two materials, but otherwise the spectra are highly similar. The spectra anneal in both materials at ~140 °C.

A model has been presented which identifies the spectra as electronic transitions from an orbital singlet ground state of a donor defect to a manifold of Coulombically bound large-orbit effective-mass excited states. The defect is deduced to be anisotropic which splits each of the $2P_0$ and $2P_{\pm1}$ lowest excited P states associated with the *isotropic* donor into three states. Transitions to these six states can account for the dominant lines observed. The differences in the spectra between the phosphorus- and arsenic-doped materials are taken to indicate that at least one group-V atom is a constituent of the defect.

This model satisfactorily accounts for the behavior of the spectra under uniaxial stress:

(i) The experiments confirm that the excited states couple primarily to the diagonal components of the stress as predicted by simple deformation-potential theory for the conduction-band minima. The uniaxial deformation potential Ξ_u is determined to be 7.2 ± 0.4 eV, in very good agreement with other estimates.

(ii) The ground state couples to off-diagonal components of stress as well, suggesting a defect symmetry of monoclinic II or lower.

Let us now consider if the defect can be identified. The obvious defect to consider first is the group-V atom-vacancy pair (E center), which has been studied in detail by EPR.[33,34] This center is believed to be the dominant defect produced in n-type float-zone-refined silicon by electron irradiation. Also the annealing temperature (~130–150 °C) agrees closely with the annealing temperature observed for the ir bands. However, the symmetry of the E center is different, i.e., monoclinic I. In addition, the E center should not have bound effective-mass states because it is believed to be negatively charged for the equilibrium state of the Fermi-level conditions of our experiment.[33,34] One other very important argument against identifying this defect as the E center is the lack of stress-induced dichroism in the ir bands. EPR studies have demonstrated that in the neutral-charged state, a strong static Jahn-Teller distortion occurs. A simple extension of the molecular-orbital model which has been so successful in understanding these defects[33–35] also predicts a Jahn-Teller distortion in the single-negative state. A Jahn-Teller distorted defect should align in the applied stress field and dichroism would therefore be observed. Confirmation of this effect for the negatively charged E center has been observed in a band at ~1.7 μ which has been identified as arising directly from the E center.[36,37]

The bands, therefore, must arise from some center other than the simple group-V atom-vacancy

pair. Unfortunately, no other defects involving group-V atoms have been identified by EPR with which we can make a direct correlation. It is possible to consider other models involving more than one vacancy with one or more group-V atoms, as well as interstitial complexes, etc. However, our ir data are not sufficient by themselves to distinguish between the large number of such possible defect configurations and we therefore feel that such speculations are not appropriate at this stage.

In this regard, it should be pointed out that the intensity of the bands is actually quite weak. Compared to the intensity of the $1S \rightarrow 2P$ transitions for the normal T_d shallow donors, our bands might be produced by $\lesssim 10^{15}$ defects. The bands may therefore arise from a rare defect in quite low concentration.

One additional clue can be mentioned. The energy difference between the average of the $2P_{\pm 1}$ lines and the average of the $2P_0$ lines in both materials is close to the value (20 meV) predicted by effective-mass theory for a center of effective charge $Z = 2$. This might be interpreted to indicate that the defect is a double donor in its first ionized state.

In order to analyze the stress behavior, we have extended the symmetry arguments of Kaplyanskii[12,13] and Runciman[14] to include the accidental degeneracy in the excited effective-mass states associated with the displaced ⟨100⟩ conduction-band minima of silicon. We have included a general table for all symmetry classes which may be useful for others in analyzing optical spectra in silicon and other similar multivalleyed semiconductors.

ACKNOWLEDGMENTS

We thank Dr. Rosa C. Young for making the annealing measurements. The major effort of James A. Chernault and James W. Westhead in developing the cold ir window (AgCl) technique is gratefully acknowledged. We also thank Dr. R. M. Chrenko and Dr. R. S. McDonald of the General Electric Research and Development Center for assistance given to us at various times. Finally we thank Arthur Tang of the General Diode Corp. for providing us with some of the silicon material used in this research.

---

*The major part of this research was supported by a Themis contract.

†Part of a Ph. D. thesis submitted to the Physics Department at Rensselaer Polytechnic Institute.

[1]G. D. Watkins, in *Proceedings of the Seventh International Conference on the Physics of Semiconductors, Paris*, 1964, edited by P. Baruch (Academic, New York, 1965), Vol. III, p. 197.

[2]E. L. Elkin and G. D. Watkins, Phys. Rev. 174, 881 (1968) (earlier references to EPR studies are cited in this paper).

[3]H. Y. Fan and A. K. Ramdas, J. Appl. Phys. 30, 1127 (1959).

[4]V. S. Vavilov, A. F. Plotnikov, and G. V. Zakhvathkin, Fiz. Tverd. Tela 1, 976 (1959) [Sov. Phys. Solid State 1, 894 (1959)].

[5]J. W. Corbett, G. D. Watkins, R. M. Chrenko, and R. S. McDonald, Phys. Rev. 121, 1015 (1961).

[6]J. C. Corelli, G. Oehler, J. F. Becker, and K. J. Eisentraut, J. Appl. Phys. 36, 1787 (1965).

[7]L. J. Cheng, J. C. Corelli, J. W. Corbett, and G. D. Watkins, Phys. Rev. 152, 761 (1966).

[8]R. E. Whan and F. L. Vook, Phys. Rev. 153, 814 (1967).

[9]F. L. Vook and H. J. Stein, in *Radiation Effects in Semiconductors*, edited by F. L. Vook (Plenum, New York, 1968), p. 99.

[10]R. C. Young, J. W. Westhead, and J. C. Corelli, J. Appl. Phys. 40, 271 (1969).

[11]A preliminary account of this work was presented by C. S. Chen, J. C. Corelli, and G. D. Watkins, Bull. Am. Phys. Soc. 14, 395 (1969).

[12]A. A. Kaplyanskii, Opt. i Spectroskopiya 16, 1031 (1964) [Opt. Spectry. (USSR) 16, 557 (1964)].

[13]A. A. Kaplyanskii, Opt. i Spectroskopiya 16, 602 (1964) [Opt. Spectry. (USSR) 16, 329 (1964)].

[14]W. A. Runciman, Proc. Phys. Soc. (London) 86, 629 (1965).

[15]R. D. Hancock and S. Edelman, Rev. Sci. Instr. 27, 1082 (1956).

[16]A. H. Kalma, Ph. D. thesis (Rensselaer Polytechnic Institute, 1968) (unpublished), available from University Microfilms Inc., Ann Arbor, Michigan.

[17]A one-component fine Epoxy powder, heat cured for 1 h at 198 °C. The epoxy is available from the Dexter Corporation, Hysol Division, Olean, N. Y. 14760.

[18]A. M. Stoneham and M. Lanoo, J. Phys. Chem. Solids 30, 1769 (1969).

[19]W. Kohn and J. M. Luttinger, Phys. Rev. 98, 915 (1955).

[20]W. Kohn, in *Solid State Physics*, edited by F. Seitz and D. Turnbull (Academic, New York, 1957), Vol. 5, p. 257.

[21]R. A. Faulkner, Phys. Rev. 184, 713 (1969).

[22]G. S. Picus, E. Burstein, and B. Henvis, J. Phys. Chem. Solids 1, 75 (1956).

[23]R. L. Aggarwal and A. K. Ramdas, Phys. Rev. 137, A602 (1965).

[24]C. Herring, Bell System Tech. J. 34, 237 (1965).

[25]C. Herring and E. Vogt, Phys. Rev. 101, 944 (1956).

[26]In this paper, we conform to the usual convention that σ is positive for tension.

[27]R. L. Aggarwal, P. Fisher, V. Mourzine, and A. K. Ramdas, Phys. Rev. 138, A882 (1965).

[28]R. L. Aggarwal and A. K. Ramdas, Phys. Rev. 146, A1246 (1965).

[29]W. E. Krag, M.I.T. Lincoln Laboratory Solid State Research Report No. 4, 1967, p. 31 (unpublished).

[30]L. T. Ho and A. K. Ramdas, Phys. Letters 32A, 23 (1970).

[31]In order to condense all symmetry classes into three entries in Table I, it was necessary to adopt a different labeling convention for the components of A for the monoclinic-II center from that of Kaplyanskii (Ref. 13). Our convention is given in Fig. 15.

[32]W. E. Krag, W. H. Kleiner, H. J. Zeiger, and S.

Fischler, J. Phys. Soc. Japan Suppl. 21, 230 (1966).
[33]G. D. Watkins and J. W. Corbett, Phys. Rev. 134, A1359 (1964).
[34]E. L. Elkin and G. D. Watkins, Phys. Rev. 174, 881 (1968).
[35]G. D. Watkins, in *Radiation Damage in Semiconductors* (Dunod, Paris, 1965), p. 97.
[36]G. D. Watkins, in *Radiation Effects in Semiconductors*, edited by F. L. Vook (Plenum, New York, 1968), p. 67.
[37]G. D. Watkins (unpublished).

PHYSICAL REVIEW B VOLUME 5, NUMBER 2 15 JANUARY 1972

Nonequilibrium Carrier Phenomena in *n*-Type InSb

Charles L. Dick, Jr. and Betsy Ancker-Johnson
Boeing Scientific Research Laboratories and University of Washington,* *Seattle*, *Washington* 98105
(Received 2 June 1971)

Four nonequilibrium carrier phenomena, namely, the hot-electron effect, injection, impact ionization, and bulk negative differential conductivity (BNDC), produce nonlinear conduction in n-InSb in a strongly interrelated manner. These interrelationships are shown in detail. The hot-electron effect causes more decrease in average conduction under most transport conditions than injection causes increase and thus injection is not so easily observed. As the electric field strength is increased into the impact ionization range which begins at $\simeq 225$ V/cm, the generation rate progressively exhibits an e^E, an $e^{1/E}$, and then an e^{1/E^2} dependence. The distribution of the carriers in energy space shifts from a peaked distribution for 225 V/cm $\lesssim E \lesssim 425$ V/cm to an isotropic distribution for $E \gtrsim 500$ V/cm. While the carriers are in a peaked distribution, the polar-optical-phonon scattering changes from small-angle scattering to large-angle as E is increased. The origin of type-S BNDC is explained, as is its temporal and spatial relationship to type-N BNDC. The S-BNDC results from the presence of copious excess carriers that are generated by impact ionization within the propagating high-field domain (HFD) associated with the Gunn effect and the N-BNDC. A low-electric-field-strength region is responsible for the S-BNDC, a region that propagates in the wake of the HFD associated with type N. A HFD in InSb makes a single transit as a result of impact ionization within the domain. The N-BNDC in n-InSb decays in typically <10 nsec, the transit time for a HFD, whereas the S-BNDC persists for several hundred nanoseconds. Radiative recombination measurements show conclusively that the S-BNDC is caused by excess carrier generation as proposed. The decay of these excess carriers is found to be characterized by two times. The faster, ~ 27 nsec, persists for typically ~ 150 nsec, a much shorter duration than the S-BNDC decay time, and is not understood at this time. However, the longer excess-carrier decay time prevails well beyond the S-BNDC disappearance, a phenomenon that is explainable by the hot-electron effect.

I. INTRODUCTION

The hot-electron effect,[1] injection,[2] impact ionization,[3–5] and bulk negative differential conductivity (BNDC)[6–8] are known nonequilibrium conduction phenomena associated with semiconductors, in particular with n-InSb. Nonequilibrium conduction refers here to any condition of nonlinear (or non-Ohmic) conduction that results when a voltage is applied to a semiconductor sample. The conduction may become nonlinear because carriers in excess of the number in thermal equilibrium with the lattice are introduced by the applied voltage. Nonlinearity may also occur because the transport properties of the charge carriers are modified by the applied field. A combination of these possibilities may also exist. Excess carriers are introduced into a semiconductor under the influence of an applied voltage by injection and/or impact ionization. The hot-electron effect influences the transport properties of electrons because of the attendant mobility reduction. BNDC can be the result of a change in the mobility of some charge carriers, or the result of the introduction of excess carriers, or a complicated combination of both of these possibilities.

These four nonequilibrium phenomena are strongly interrelated in n-InSb, a fact complicating their study, particularly because these phenomena occur on extremely short time scales. The short time scales require rather sophisticated diagnostic techniques. The measurements are further complicated by the fact that the lattice is held at a low temperature, 77 K, unless stated otherwise. This temperature is chosen because it nearly maximizes both carrier mobilities in InSb and is conveniently attained.

This work shows the interrelationship of these four nonequilibrium phenomena in n-InSb and gives new information about each, including a new effect: a temporal and spatial relationship between type-N and type-S BNDC.[8]